Supporting Information for

Quantifying effects of second-sphere cationic groups on redox properties of dimolybdenum quadruple bonds

S. M. Supundrika Subasinghe and Neal P. Mankad*
Department of Chemistry, University of Illinois at Chicago, 845 W. Taylor St., Chicago, IL 60607, USA

*Corresponding author: npm@uic.edu

Table of Contents

1. Experimental Section

1.1 General Considerations

All experimental manipulations were conducted under a dry nitrogen atmosphere employing glovebox techniques. Reaction solvents were subjected to drying procedures using a Glass Contour Solvent System supplied by Pure Process Technology, LLC. Solution NMR spectra were recorded in deuterated solvents. The deuterated solvents were degassed and dried over 3-Å molecular sieves. The syntheses of *cis*-$Mo_2(DAniF)_2(MeCN)_4$ and $Mo_2(DAniF)(MeCN)_6$ followed previously reported procedures from the literature.[1] Unless explicitly stated, all other chemicals were obtained from commercial sources and used without further purification.

Proton (^1H), carbon ($^{13}C\{^1H\}$), and lithium (^7Li) nuclear magnetic resonance (NMR) spectra were acquired using Bruker Avance DPX-500 or DPX-400 MHz spectrometers for room-temperature spectra and using a Bruker Avance III HD 500 MHz spectrometer for variable-temperature spectra. Chemical shifts were referenced to the residual solvent signals for ^1H and $^{13}C\{H\}$ spectra (CD_3CN at 1.94 and 118.26 ppm, respectively) and to an external 9.7 M LiCl sample in D_2O (0 ppm) for ^7Li spectra. High-resolution mass spectroscopy (HRMS) was performed by the School of Chemical Sciences Mass Spectrometry Laboratory (MSL) in University of Illinois Urbana-Champaign. In this study, HRMS data was obtained using electrospray ionization (ESI) method in positive mode. We were unable to obtain satisfactory elemental analysis data after repeated attempts, so NMR spectra are provided as indications of purity and HRMS data for verification of empirical formulas.

All electrochemical analyses were conducted within a glovebox filled with nitrogen gas. The supporting electrolytes used were tetrabutylammonium hexafluorophosphate ($[Bu_4N][PF_6]$) of electrochemical grade, tetrabutylammonium trifluoromethanesulfonate ($[Bu_4N][OTf]$) of electrochemical grade, and tetrabutylammonium tetrakis(pentafluorophenyl)borate ($[Bu_4N][B(C_6F_5)_4]$) that was synthesized by literature procedures.[2] All the electrolytes were dried at 100 °C for 24 h before utilization. Cyclic voltammetry measurements were performed using a BioLogic VSP potentiostat in a three-electrode electrochemical cell configuration. The cell consisted of a BASi glassy carbon working electrode (0.07 cm^2), a BASi Ag/Ag^+ quasi-reference electrode containing 0.01 M $Ag(NO)_3$ in acetonitrile, and a platinum wire counter electrode (23 cm, ALS). Cyclic voltammograms were collected in both acetonitrile and acetone solvents, which were reagent grade. All experiments were carried out at a scan rate of 100 mV s^{-1} in an electrolyte containing 1.5 mM of the target complex and 0.1 M of electrolyte.

1.2 Synthesis Procedures

1.2.1 Preparation of Li^+ DMG

A mixture of lithium methoxide (184.1 mg, 4.84 mmol) and MeOH (5 mL) was added to a scintillation vial containing DMG (500 mg, 4.84 mmol). The reaction mixture was stirred overnight. The reaction mixture was filtered through Celite, and the solvent was removed under the vacuum.
^1H NMR (400 MHz, CD_3OD): δ 2.96 (s, 1H, DMG CH_2), 2.30 (s, 6H, DMG NCH_3).
^7Li NMR (156 MHz, CD_3OD): δ -2.93.

1.2.2 Preparation of compound 1

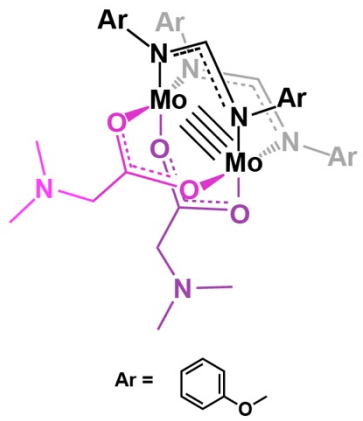

To a scintillation vial, Li^+ DMG (19.2 mg, 0.179 mmol) was added, followed by the slow dropwise addition of a solution of [*cis*-$Mo_2(DAniF)_2(CH_3CN)_4](BF_4)_2$ (60.3 mg, 0.058 mmol) in acetonitrile (5 mL). The reaction mixture was stirred for 2 h at room temperature. After the 2 h reaction period, the mixture was filtered through Celite, and the resulting filtrate was concentrated to 1 mL. Subsequently, diethyl ether (5 mL) was added, resulting in the observation of a yellow precipitate. The yellow precipitate was isolated by filtration, thoroughly dried *in vacuo*.

^{1}H NMR (500 MHz, CD_3CN): δ 8.50 (s, 2H, DAniF N-C*H*-N), 6.69 (d, *J* = 8.8 Hz, 8H, DAniF aromatic *H*), 6.69 (d, *J* = 8.8 Hz, 8H, DAniF aromatic *H*), 4.46 (s, 4H, DMG CH_2), 3.69 (s, 12H, DAniF OCH_3), 3.03 (s, 12H, DMG NCH_3).
^{13}C NMR (126 MHz, CD_3CN): δ 159.6 (N-*C*H-N), 157.6 (Ar), 143.5 (Ar), 125.1 (Ar), 114.8 (Ar), 61.7 (C-CH_2), 56.0 (OCH_3), 45.2 ($N(CH_3)_2$). *Note:* signal for the $^-$O-C=O group could not be observed.
HRMS (ESI/TOF) *m/z*: $[M+2Li+2CH_3CN]^{+2}$ Calcd for $C_{42}H_{52}Mo_2N_8O_8Li_2$ 1003.235, found 1003.150

1.2.3 Preparation of compound 2

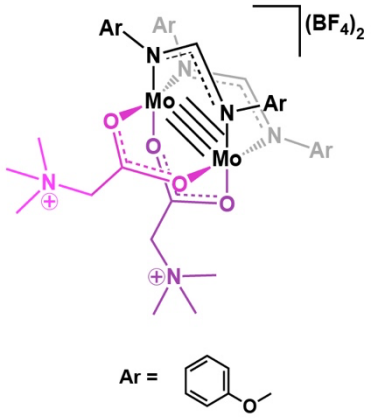

To a scintillation vial, TMG (18.1 mg, 0.155 mmol) was added, followed by the slow dropwise addition of a solution of [*cis*-$Mo_2(DAniF)_2(CH_3CN)_4](BF_4)_2$ (52.9 mg, 0.051 mmol) in acetonitrile (5 mL). The reaction mixture was stirred for 2 h at room temperature. After the 2 h reaction period, the mixture was filtered through Celite, and the resulting filtrate was concentrated to 1 mL. Subsequently, diethyl ether (5 mL) was added, resulting in the observation of a yellow precipitate. The yellow precipitate was isolated by filtration, thoroughly dried *in vacuo*.

^{1}H NMR (400 MHz, CD_3CN): δ 8.54 (s, 2H, DAniF N-C*H*-N), 6.68 (s, 16H, DAniF aromatic *H*), 4.62 (s, 4H, TMG CH_2), 3.69 (s, 12H, DAniF OCH_3), 3.35 (s, 18H, TMG NCH_3).
^{13}C NMR (101 MHz, CD_3CN): δ 159.7 (N-*C*H-N), 157.1 (Ar), 143.7 (Ar), 123.5 (Ar), 115.4 (Ar), 66.2 (C-CH_2), 56.0 (OCH_3), 45.2 ($N(CH_3)_2$). *Note:* signal for the $^-$O-C=O group could not be observed.
HRMS (ESI/TOF) *m/z*: $[M-CH_3+2CH_3CN]^+$ Calcd for $C_{43}H_{55}Mo_2N_8O_8$ 1004.224, found 1004.149

1.2.4 Preparation of compound 3

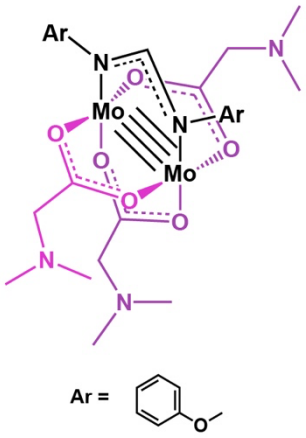

To a scintillation vial, Li^+ DMG (19.5 mg, 0.179 mmol) was added, followed by the slow dropwise addition of a solution of $[Mo_2(DAniF)(CH_3CN)_6](BF_4)_3$ (33.1 mg, 0.035 mmol) in acetonitrile (5 mL). The reaction mixture was stirred for 12 h at room temperature. After the 12 h reaction period, the mixture was filtered through Celite, and the resulting filtrate was concentrated to 1 mL. Subsequently, diethyl ether (5 mL) was added, resulting in the observation of a yellow precipitate. The yellow precipitate was isolated, thoroughly dried *in vacuo*.

^{1}H NMR (400 MHz, CD_3CN): δ 8.56 (s, 1H, DAniF N-C*H*-N), 7.16 – 6.66 (m, 8H, DAniF aromatic *H*), 4.40 (s, 6H, DMG CH_2), 3.73 (s, 6H, DAniF OCH_3), 2.92 (s, 18H, DMG NCH_3).
^{13}C NMR (101 MHz, CD_3CN): δ 162.2 (N-*C*H-N), 158.0 (Ar), 143.1 (Ar), 125.65 (Ar), 114.8 (Ar), 61.08 (C-*C*H_2), 56.1 (O*C*H_3), 45.2 (N(*C*H_3)$_2$). *Note:* signal for the $^-$O-C=O group could not be observed.
HRMS (ESI/TOF) *m/z*: $[M+Li]^+$ Calcd for $C_{27}H_{39}Mo_2N_5O_8Li$ 760.086, found 760.025

1.2.5 Preparation of compound 4

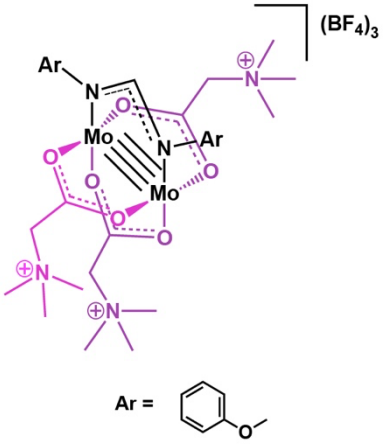

To a scintillation vial, TMG (22.5 mg, 0.193 mmol) was added, followed by the slow dropwise addition of a solution of $[Mo_2(DAniF)(CH_3CN)_6](BF_4)_3$ (35.6 mg, 0.039 mmol) in acetonitrile (5 mL)). The reaction mixture was stirred for 12 h at room temperature. After the 12 h reaction period, the mixture was filtered through Celite, and the resulting filtrate was concentrated to 1 mL. Subsequently, diethyl ether (5 mL) was added, resulting in the observation of a yellow precipitate. The yellow precipitate was isolated, thoroughly dried *in vacuo*.

^{1}H NMR (400 MHz, CD_3CN): δ 8.66 (s, 1H, DAniF N-C*H*-N), 7.02 – 6.68 (m, 8H, DAniF aromatic *H*), 4.30 (s, 6H, TMG CH_2), 3.72 (s, 6H, DAniF OCH_3), 3.26 (s, 27H, TMG NCH_3).
^{13}C NMR (101 MHz, CD_3CN): δ 161.5 (N-*C*H-N), 157.0 (Ar), 142.2 (Ar), 124.3 (Ar), 113.9 (Ar), 66.1 (C-*C*H_2), 55.1 (O*C*H_3), 53.6 (N(*C*H_3)$_2$). *Note:* signal for the $^-$O-*C*=O group could not be observed.
HRMS (ESI/TOF) *m/z*: $[M-2CH_3+CH_3CN]^+$ Calcd for $C_{30}H_{45}Mo_2N_6O_8$ 810.151, found 810.076

1.3 Experimental Data (NMR and MS)

1.3.1 NMR and mass-spec spectra for compound 1

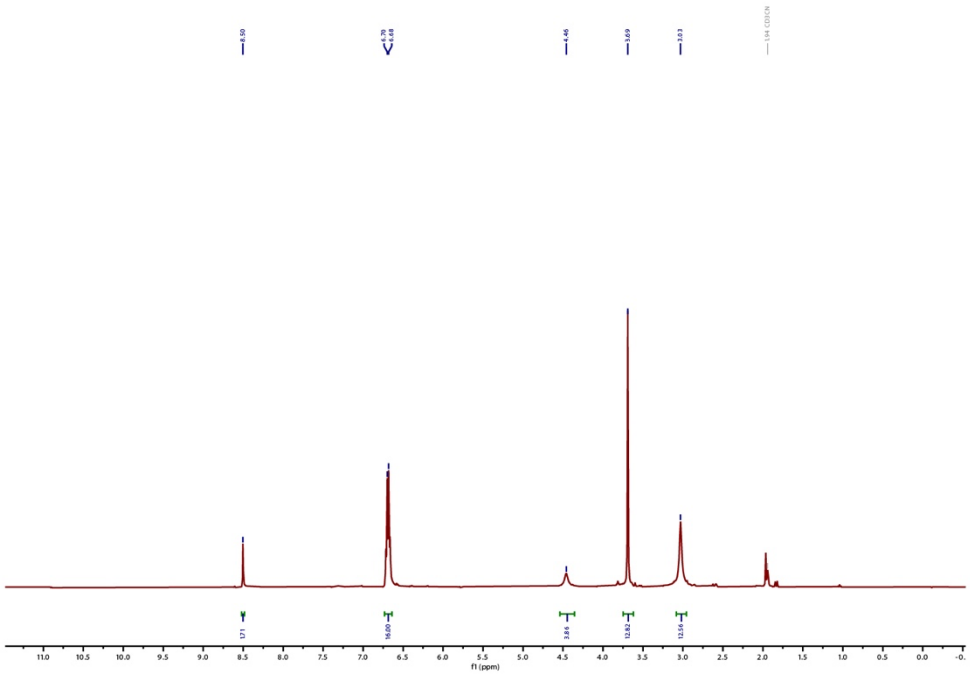

Figure S1. ^{1}H NMR spectrum of **1** at 298 K in CD3CN

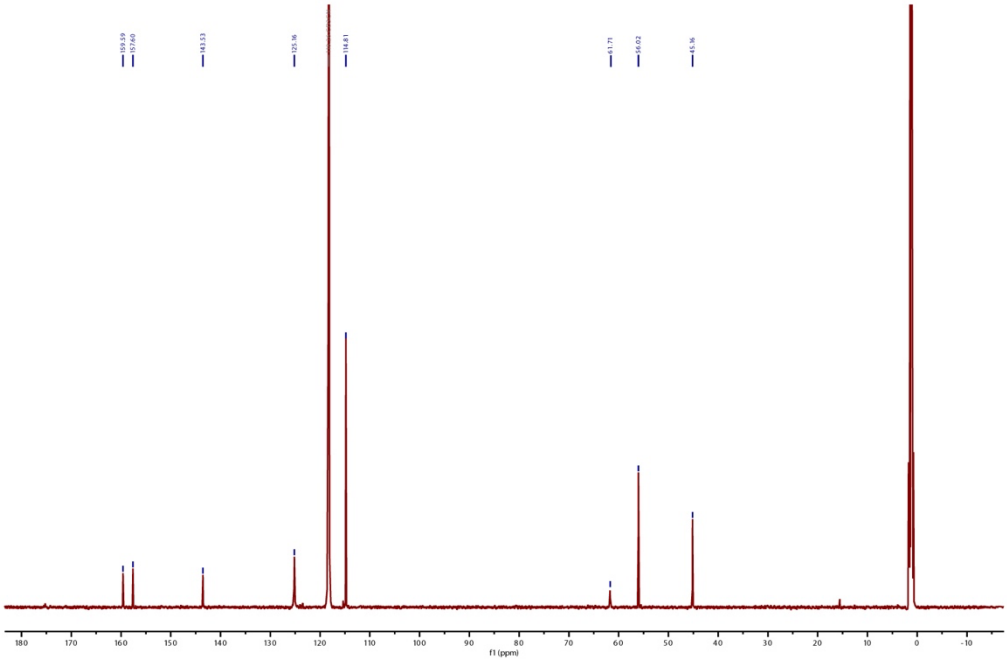

Figure S2. $^{13}C\{^{1}H\}$ NMR spectrum of **1** at 298 K in CD3CN

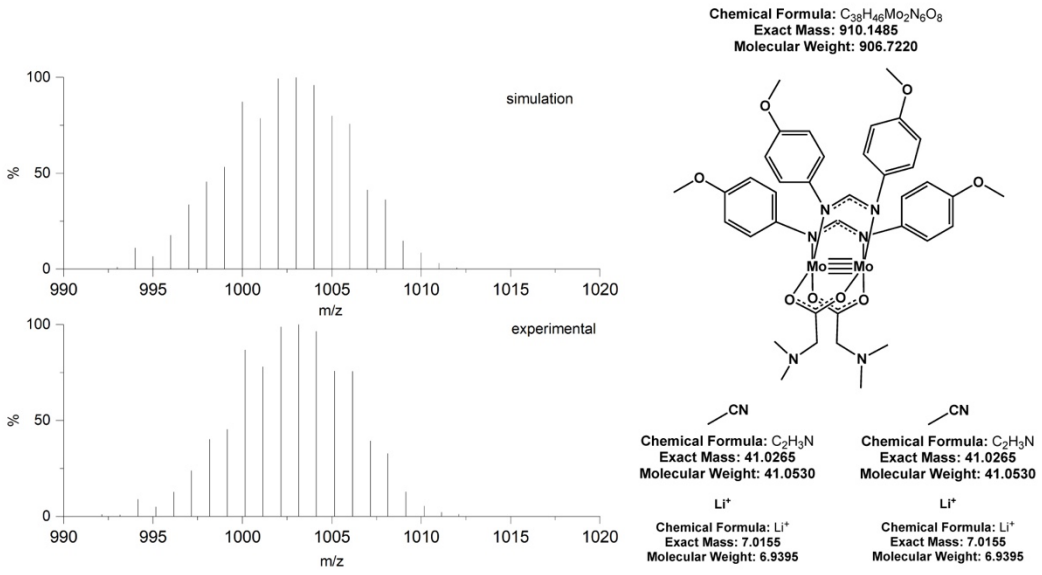

Figure S3. Comparison between experimental *vs.* simulated isotope pattern observed for **1** by ESI-MS

1.3.2 NMR and mass-spec spectra for compound 2

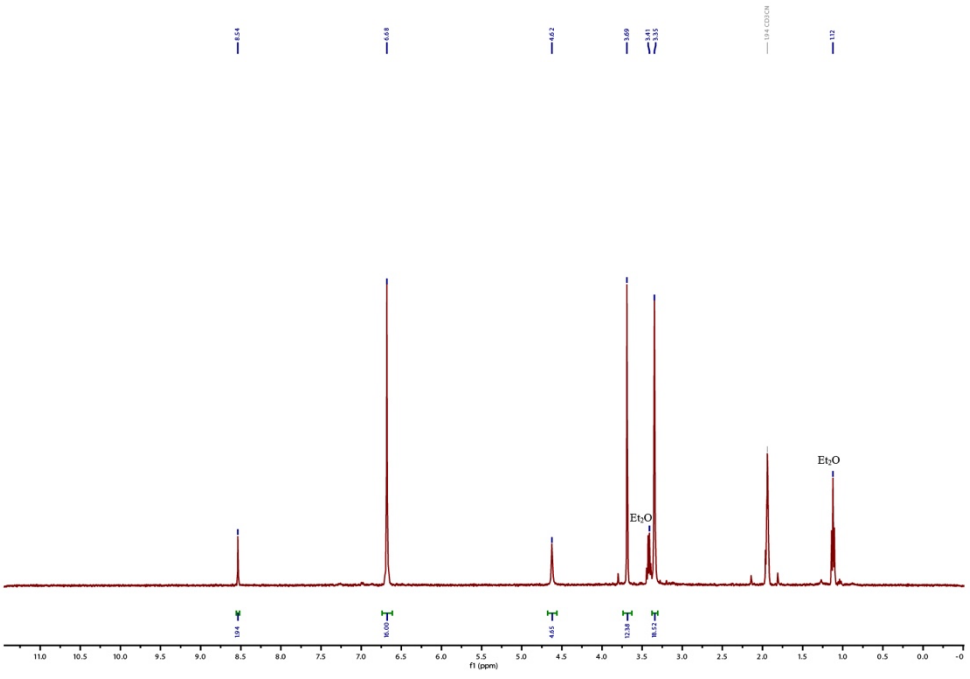

Figure S4. ^{1}H NMR spectrum of **2** at 298 K in CD3CN

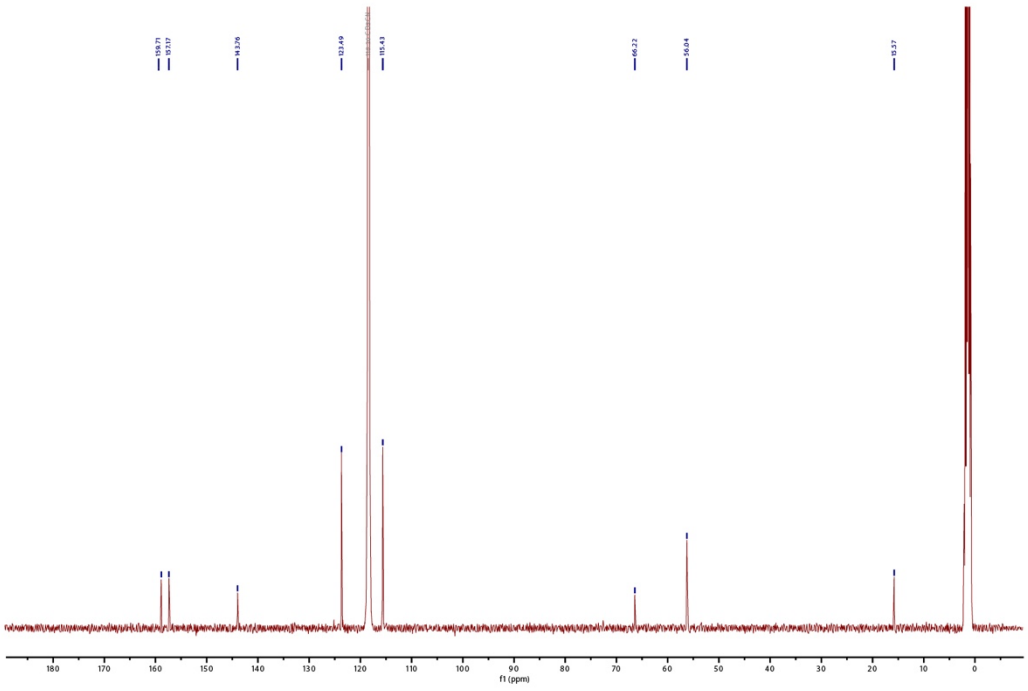

Figure S5. $^{13}C\{^{1}H\}$ NMR spectrum of **2** at 298 K in CD3CN

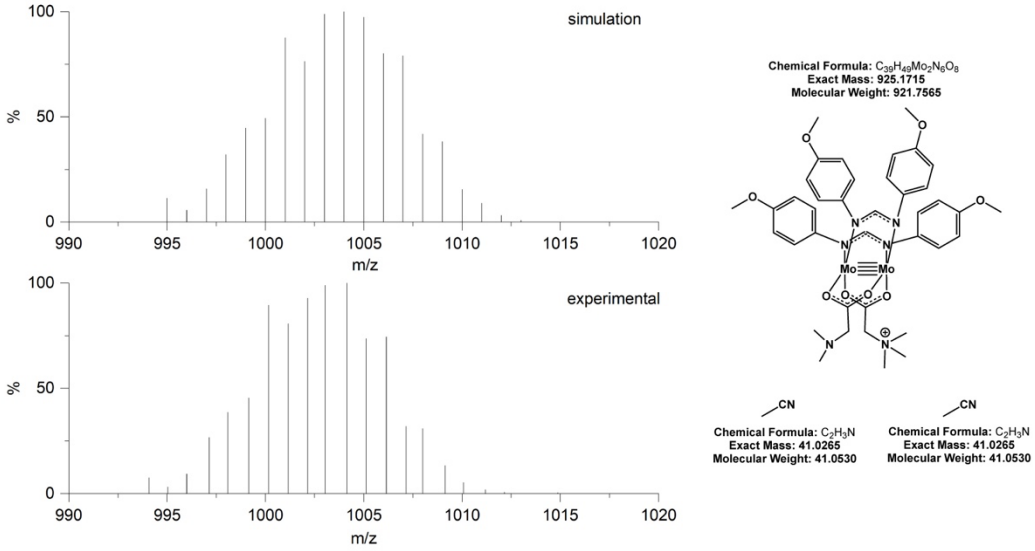

Figure S6. Comparison between experimental *vs.* simulated isotope pattern observed for **2** by ESI-MS

1.3.3 NMR and mass-spec spectra for compound 3

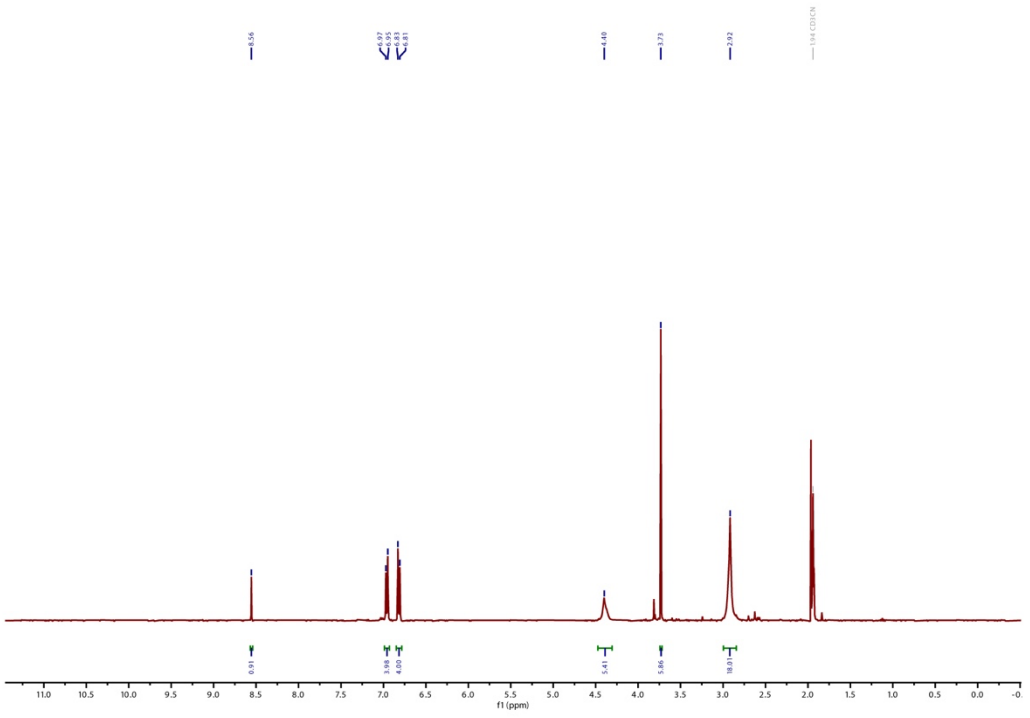

Figure S7. ^{1}H NMR spectrum of **3** at 298 K in CD3CN

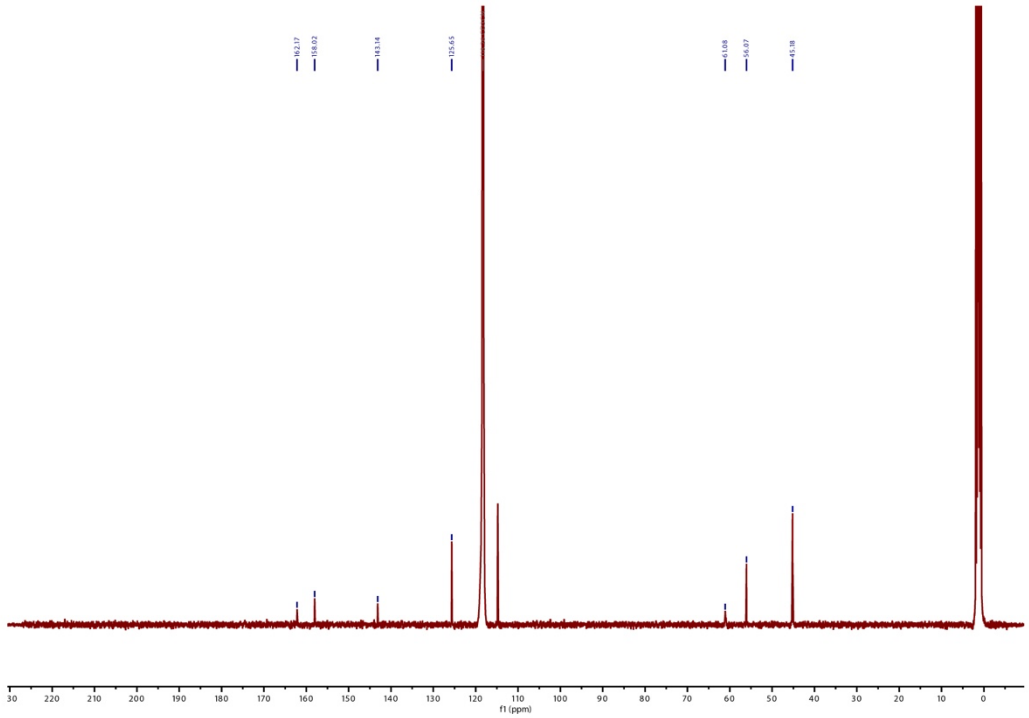

Figure S8. ^{13}C{^{1}H} NMR spectrum of **3** at 298 K in CD3CN

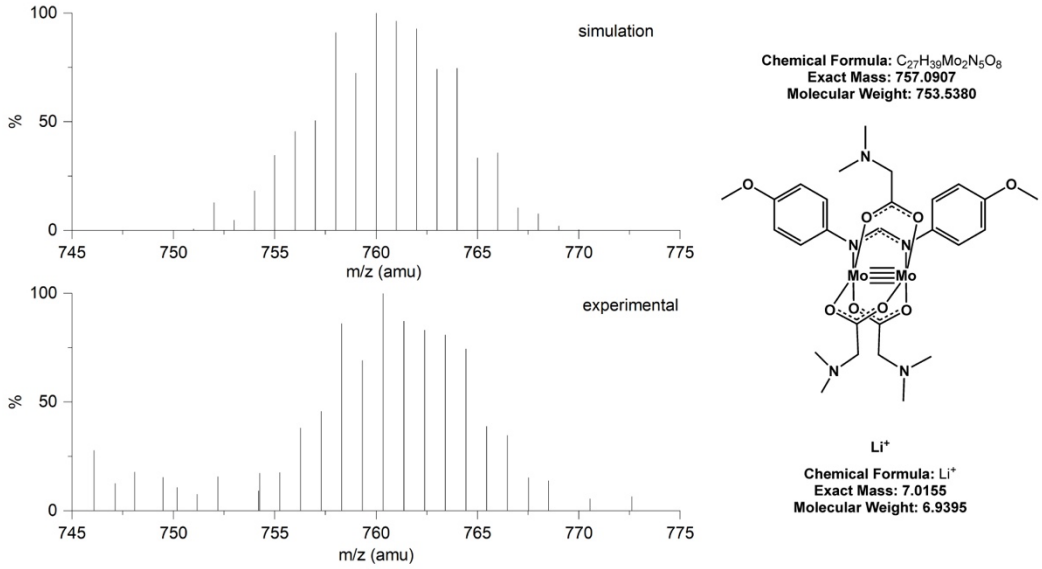

Figure S9. Comparison between experimental *vs.* simulated isotope pattern observed for **3** by ESI-MS

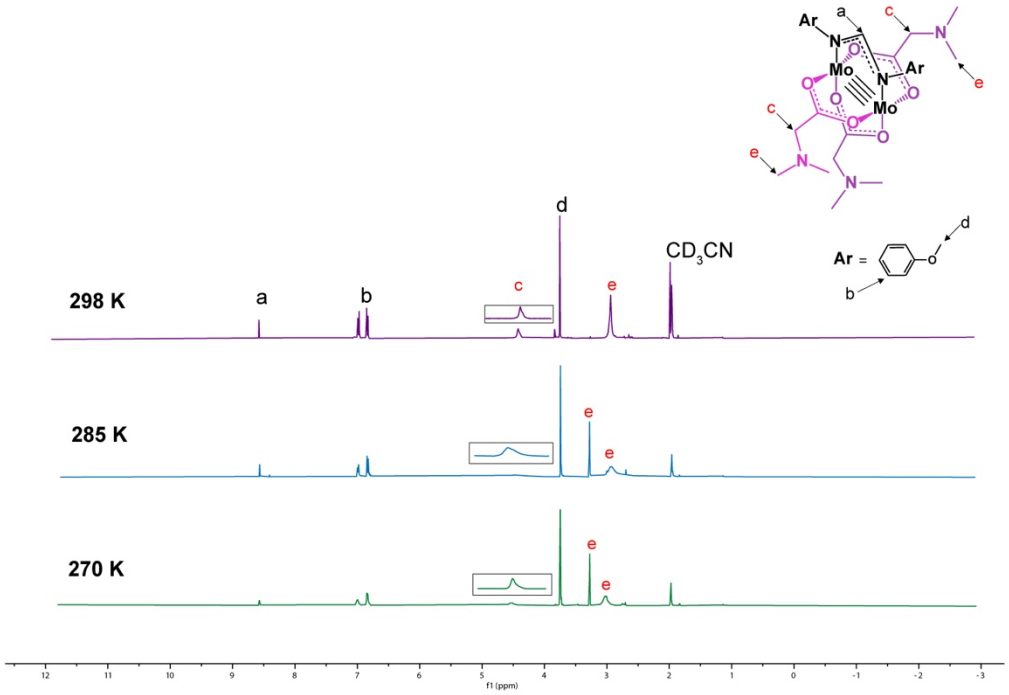

Figure S10. ^{1}H NMR spectra for **3** at different temperatures

1.3.4 NMR and mass-spec spectra for compound 4

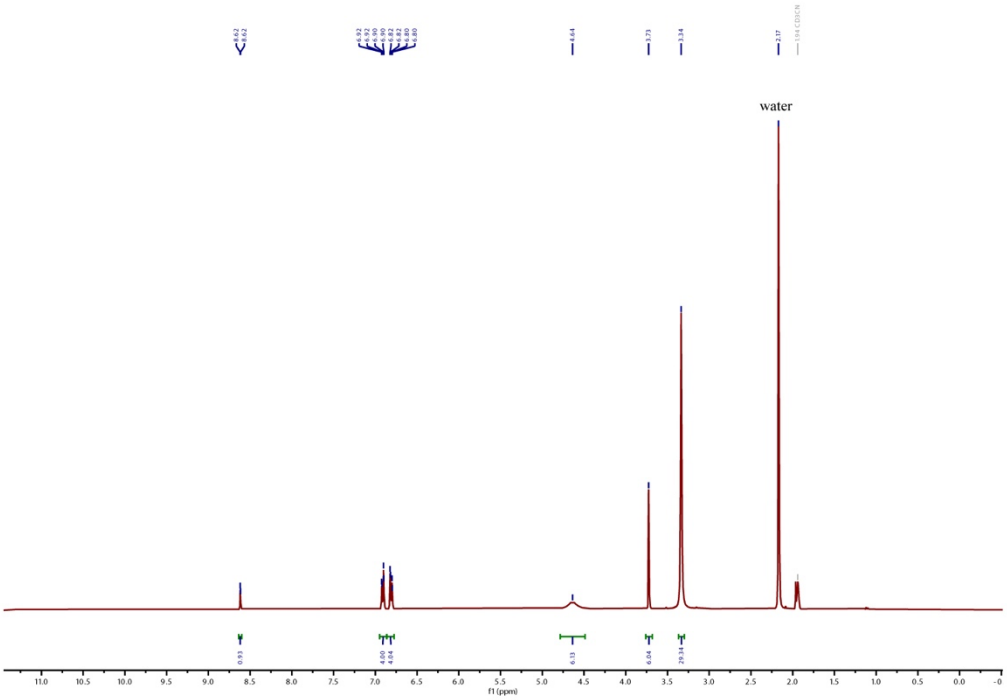

Figure S11. ^{1}H NMR spectrum of **4** at 298 K in CD3CN

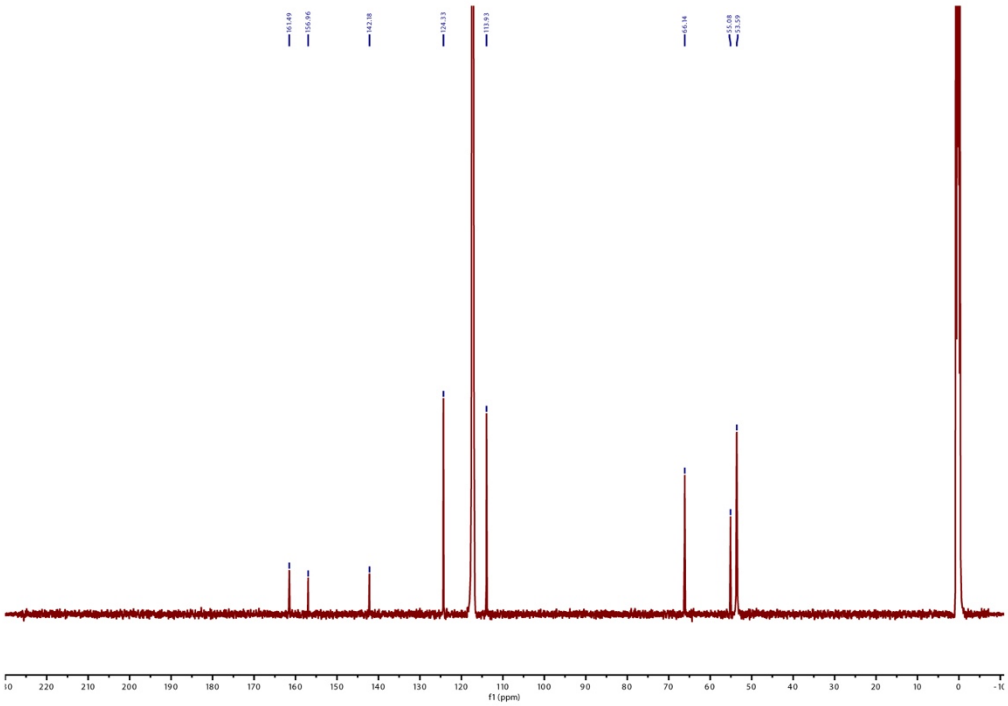

Figure S12. ^{13}C{^{1}H} NMR spectrum of **4** at 298 K in CD3CN

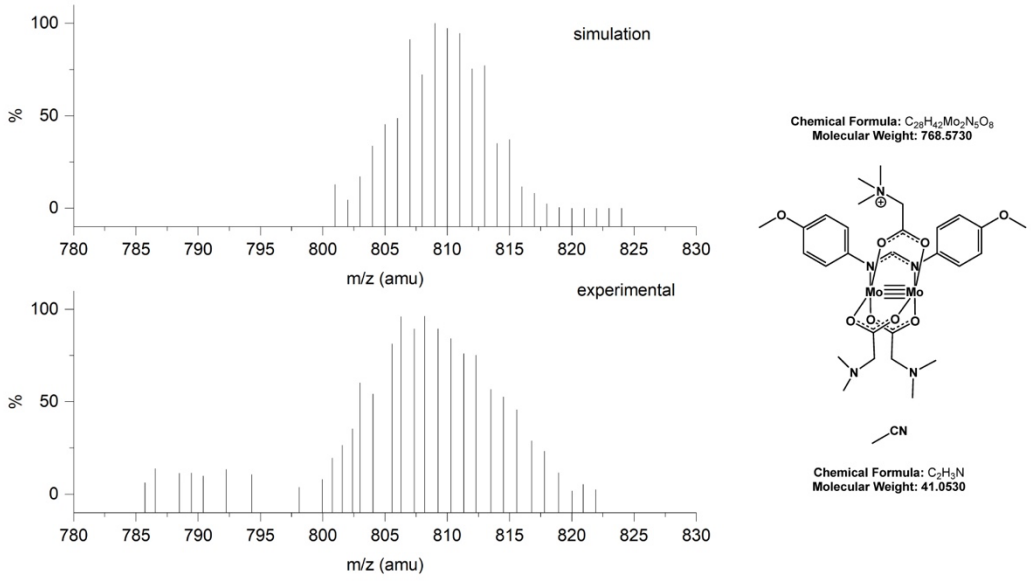

Figure S13. Comparison between experimental *vs.* simulated isotope pattern observed for **4** by ESI-MS

1.4 Electrochemistry Experimental Data

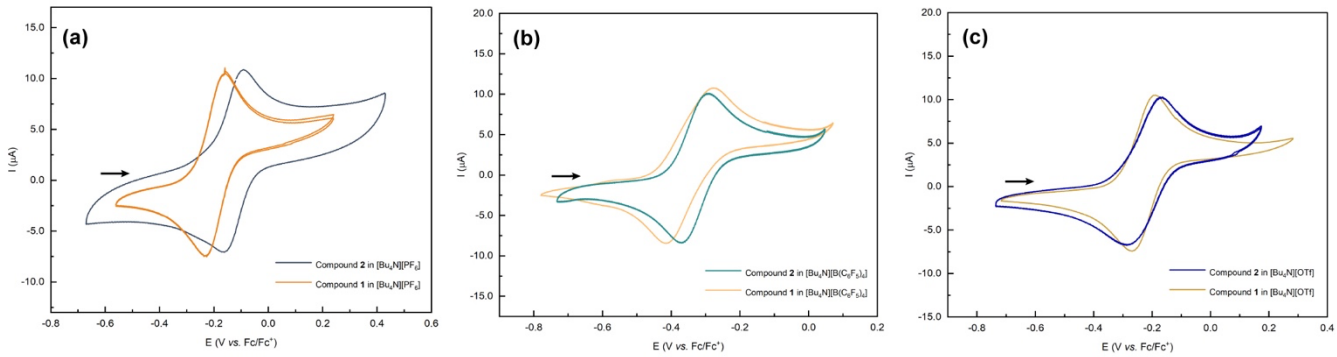

Figure S14. Cyclic voltammograms for **1** and **2** (1.5 mM) at 100 mV s^{-1} in (a) 0.1 M $[Bu_4N][PF_6]$ (b) 0.1 M $[Bu_4N][B(C_6F_5)_4]$ (c) 0.1 M $[Bu_4N][OTf]$ in CH_3CN.

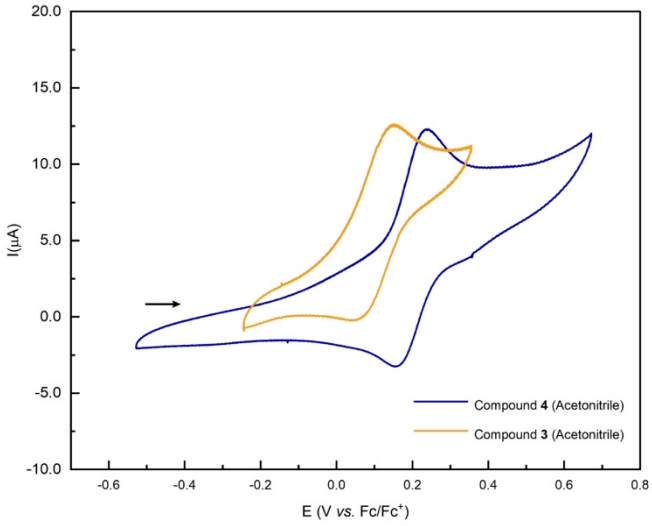

Figure S15. Cyclic voltammograms for **3** and **4** (1.5 mM) at 100 mV s^{-1} in 0.1 M $[Bu_4N][PF_6]$ in CH_3CN

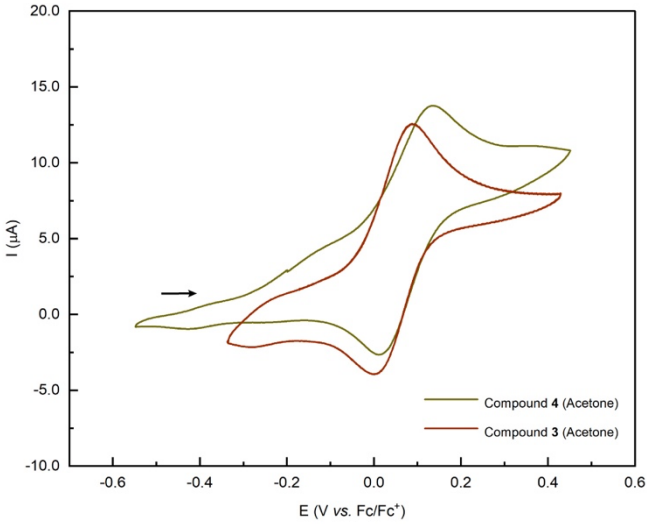

Figure S16. Cyclic voltammograms for **3** and **4** (1.5 mM) at 100 mV s^{-1} in 0.1 M $[Bu_4N][PF_6]$ in acetone

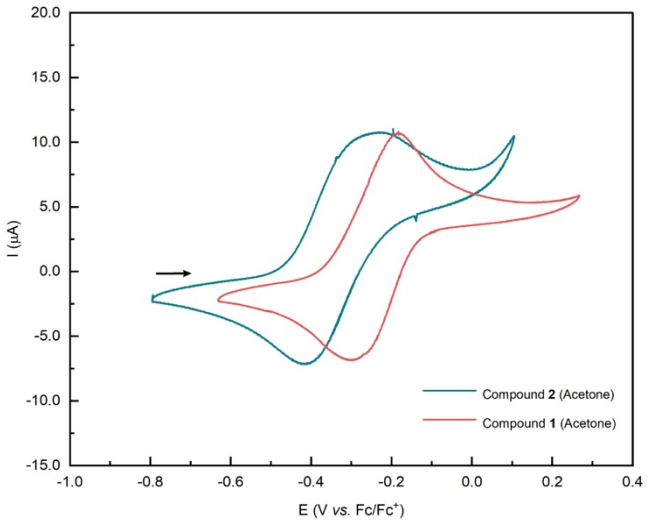

Figure S17. Cyclic voltammograms for **1** and **2** (1.5 mM) at 100 mV s^{-1} in 0.1 M $[Bu_4N][PF_6]$ in acetone

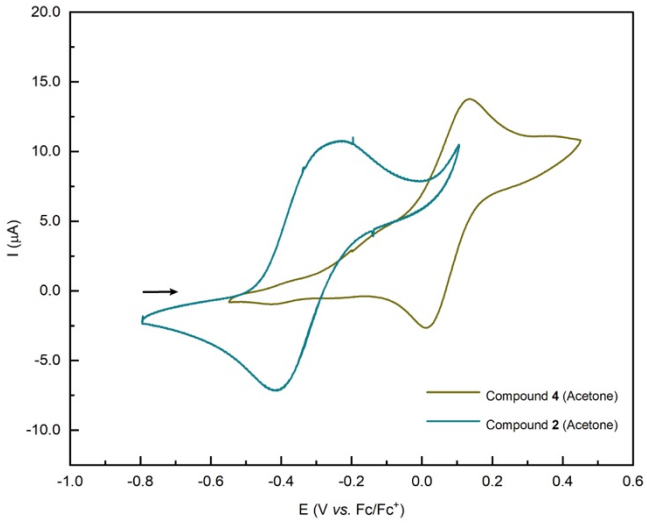

Figure S18. Cyclic voltammograms for **2** and **4** (1.5 mM) at 100 mV s^{-1} in 0.1 M $[Bu_4N][PF_6]$ in acetone

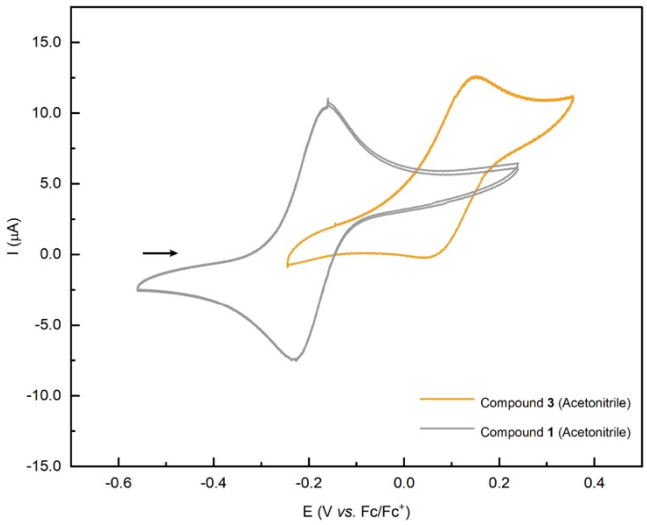

Figure S19. Cyclic voltammograms for **1** and **3** (1.5 mM) at 100 mV s^{-1} in 0.1 M $[Bu_4N][PF_6]$ in MeCN

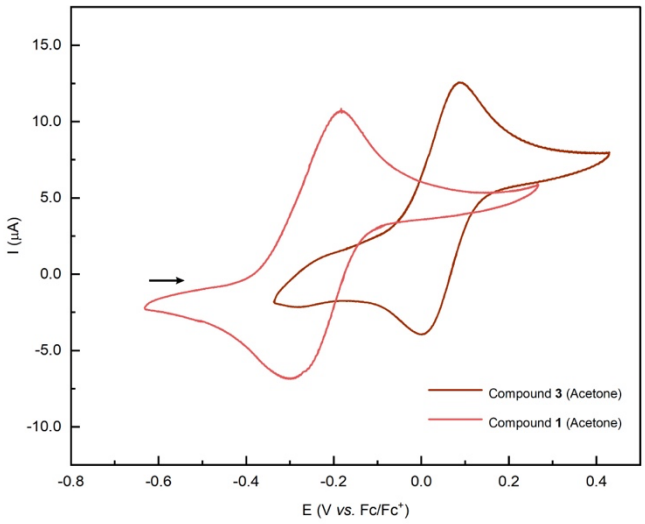

Figure S20. Cyclic voltammograms for **1** and **3** (1.5 mM) at 100 mV s^{-1} in 0.1 M $[Bu_4N][PF_6]$ in acetone

Here, we have presented the constants incorporated to calculate the shift of $E_{1/2}$.

$V = \frac{1}{4\pi\epsilon r} q \; ; \epsilon = \varepsilon_{\circ} K$ K = dielectric constant $\varepsilon_{\circ}$ = vacuum permittivity

$\boldsymbol{\pi}$	3.1416
$\boldsymbol{\varepsilon_{\circ}}$	8.854×10^{-12} Fm^{-1}
$\boldsymbol{K}$	37.5 (MeCN)
$\boldsymbol{r}$	5.1×10^{-12} m
Elementary charge	1.602×10^{-19} C

1.5 Computational Analysis

Gaussian 16 (Revision B.01)[3] was employed for density functional theory (DFT) calculations. The geometries were optimized without imposing symmetry constraints, utilizing the PBE0 hybrid functional,[4] also referred to as PBE1PBE in Gaussian. Non-relativistic core Hamiltonians and an ultrafine integration grid were utilized in the process. The geometry optimization was conducted using a triple-ζ split valence basis set with a single set of polarization functions, namely def2-TZVP. For the Mo atom, we employed the correlation-consistent polarized valence triple-ζ basis set (cc-PVTZ).[5]. Grimme's empirical dispersion correction[6] (specifically, the D3 version) was employed in order to incorporate empirical dispersion effects into all DFT functionals. Additionally, solvent effects were considered by applying the SMD[7] solvation model with default acetonitrile parameters. The analysis of vibrational frequencies verified that all identified stationary points were correctly categorized as minima on the potential energy surface without any imaginary frequencies. The open-source MultiWFN (version 3.8)[8] program was used to calculate and visualize partial atomic charges by the Hirschfeld method.[9]

Ligand	Atom number	Charge calculation method
		Hirschfeld
DMG	4 O	-0.493
	7 O	-0.445
TMG	4 O	-0.403
	6 O	-0.451

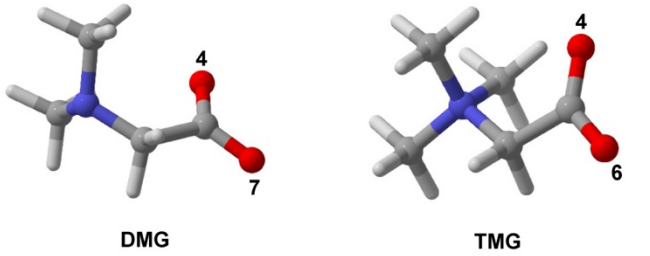

Figure S21. Partial atomic charges on oxygen atoms in DMG and TMG ligands

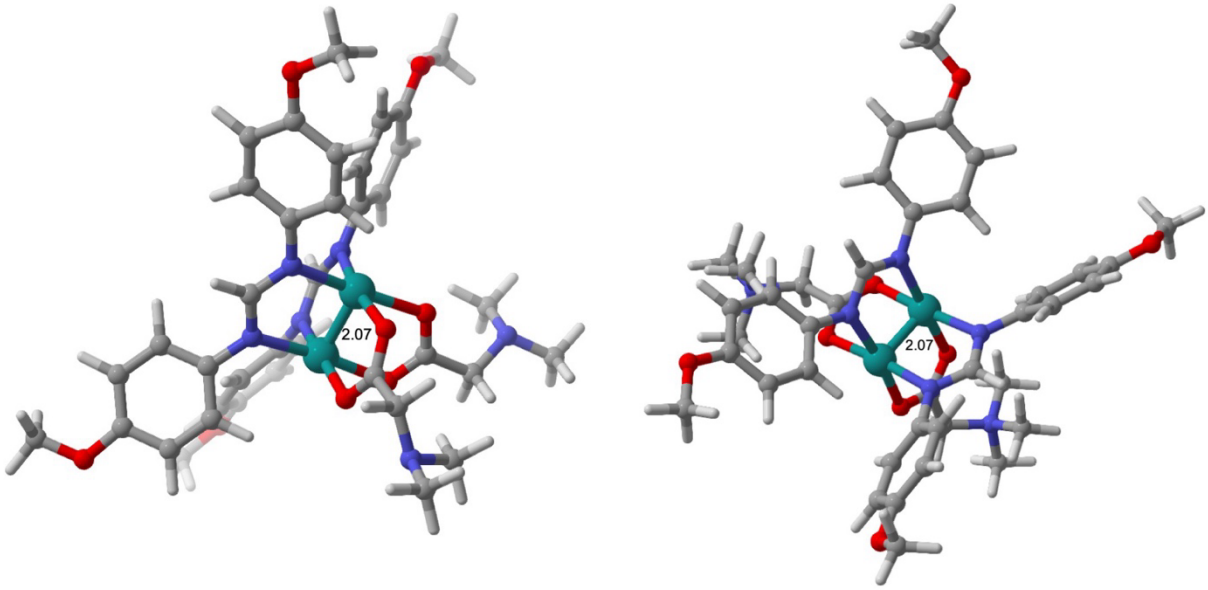

Figure S22. calculated Mo≡Mo distances for **1** and **2** in Å

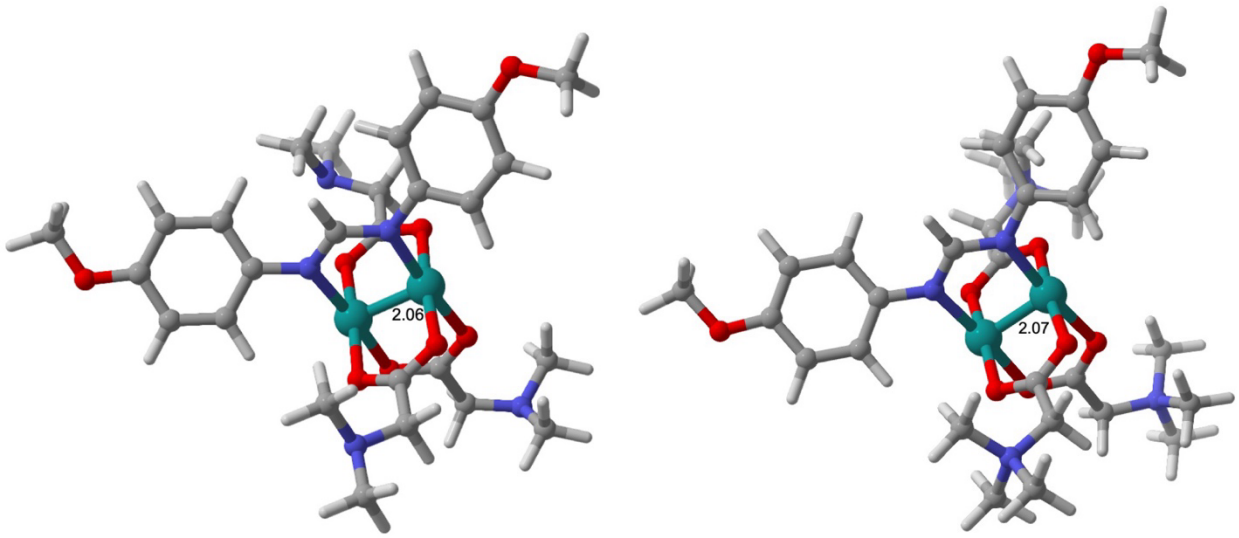

Figure S23. calculated Mo≣Mo distances for **3** and **4** in Å

In addition to analyzing the optimized structures, we also looked at the HOMO/LUMO Gibbs free energy gaps from DFT calculations. While there was no correlation found between $E_{1/2}$ and HOMO/LUMO gap, we do find it noteworthy that the difference in HOMO/LUMO gap between the neutral bis- and tris(DMG) complexes mirrors that between the polycationic bis- and tris(TMG) complexes (see **Figure S24**). This provides us with additional confidence that the charged groups do not significantly impact the primary coordination sphere, i.e., the donor/acceptor properties of the carboxylates.

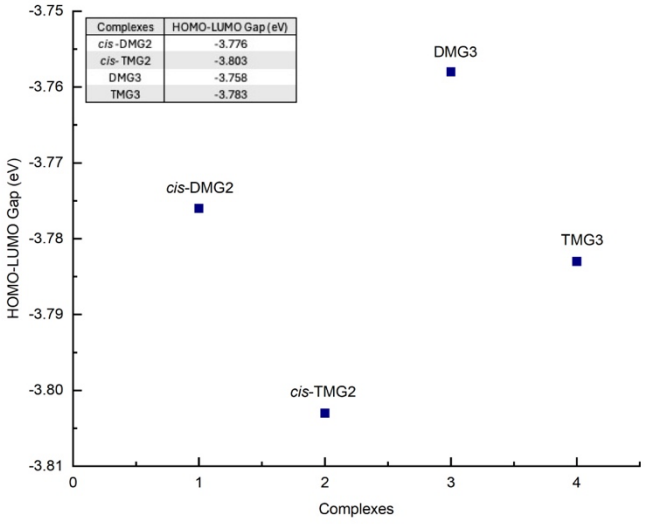

Figure S24. The difference in HOMO-LUMO gap of the optimized complexes

2. References

(1) Chisholm, M. H.; Cotton, F. A.; Daniels, L. M.; Folting, K.; Huffman, J. C.; Iyer, S. S.; Lin, C.; Macintosh, A. M.; Murillo, C. A. Compounds in Which the Mo24+ Unit Is Embraced by One, Two or Three Formamidinate Ligands Together with Acetonitrile Ligands. *J. Chem. Soc., Dalton Trans.* **1999**, No. 9, 1387–1392. https://doi.org/10.1039/a900389d.

(2) Barrière, F.; Geiger, W. E. Use of Weakly Coordinating Anions to Develop an Integrated Approach to the Tuning of ΔE1/2 Values by Medium Effects. *J. Am. Chem. Soc.* **2006**, *128* (12), 3980–3989. https://doi.org/10.1021/ja058171x.

(3) Frisch, M. J.; Trucks, G. W.; Schlegel, H. B.; Scuseria, G. E.; Robb, M. A.; Cheeseman, J. R.; Scalmani, G.; Barone, V.; Petersson, G. A.; Nakatsuji, H.; Li, X.; Caricato, M.; Marenich, A. V.; Bloino, J.; Janesko, B. G.; Gomperts, R.; Mennucci, B.; Hratchian, H. P.; Ortiz, J. V.; Izmaylov, A. F.; Sonnenberg, J. L.; Williams; Ding, F.; Lipparini, F.; Egidi, F.; Goings, J.; Peng, B.; Petrone, A.; Henderson, T.; Ranasinghe, D.; Zakrzewski, V. G.; Gao, J.; Rega, N.; Zheng, G.; Liang, W.; Hada, M.; Ehara, M.; Toyota, K.; Fukuda, R.; Hasegawa, J.; Ishida, M.; Nakajima, T.; Honda, Y.; Kitao, O.; Nakai, H.; Vreven, T.; Throssell, K.; Montgomery Jr., J. A.; Peralta, J. E.; Ogliaro, F.; Bearpark, M. J.; Heyd, J. J.; Brothers, E. N.; Kudin, K. N.; Staroverov, V. N.; Keith, T. A.; Kobayashi, R.; Normand, J.; Raghavachari, K.; Rendell, A. P.; Burant, J. C.; Iyengar, S. S.; Tomasi, J.; Cossi, M.; Millam, J. M.; Klene, M.; Adamo, C.; Cammi, R.; Ochterski, J. W.; Martin, R. L.; Morokuma, K.; Farkas, O.; Foresman, J. B.; Fox, D. J. Gaussian 16 Rev. B.01, 2016.

(4) Perdew, J. P.; Burke, K.; Ernzerhof, M. Generalized Gradient Approximation Made Simple. *Phys. Rev. Lett.* **1996**, *77* (18), 3865–3868. https://doi.org/10.1103/PhysRevLett.77.3865.

(5) Woon, D. E.; Dunning, T. H., Jr. Gaussian Basis Sets for Use in Correlated Molecular Calculations. V. Core-valence Basis Sets for Boron through Neon. *The Journal of Chemical Physics* **1995**, *103* (11), 4572–4585. https://doi.org/10.1063/1.470645.

(6) Grimme, S.; Antony, J.; Ehrlich, S.; Krieg, H. A Consistent and Accurate Ab Initio Parametrization of Density Functional Dispersion Correction (DFT-D) for the 94 Elements H-Pu. *The Journal of Chemical Physics* **2010**, *132* (15), 154104. https://doi.org/10.1063/1.3382344.

(7) Marenich, A. V.; Cramer, C. J.; Truhlar, D. G. Universal Solvation Model Based on Solute Electron Density and on a Continuum Model of the Solvent Defined by the Bulk Dielectric Constant and Atomic Surface Tensions. *J. Phys. Chem. B* **2009**, *113* (18), 6378–6396. https://doi.org/10.1021/jp810292n.

(8) Lu, T.; Chen, F. Multiwfn: A Multifunctional Wavefunction Analyzer. *Journal of Computational Chemistry* **2012**, *33* (5), 580–592. https://doi.org/10.1002/jcc.22885.

(9) Hirshfeld, F. L. Bonded-Atom Fragments for Describing Molecular Charge Densities. *Theoretica chimica acta* **1977**, *44*, 129–138.